Elastic–plastic analysis of indentation damage: cyclic loading of copper

Y. YOKOUCHI*, I. G. GREENFIELD, T.-W. CHOU, E. B. ITURBE
Materials and Metallurgy Faculty, College of Engineering, University of Delaware, Newark, Delaware 19711, USA

This is the second in a two-paper series examining the elastic–plastic deformation of a metallic target material under repeated impact. This paper examines the effect of statically cyclic loading on copper and numerical calculations have been performed up to ten cycles. The extent of the loading phase in each cycle is specified by a constant external work done by the indenter. The deformed configuration of the target material, the locus of material flow, and elastic–plastic boundaries due to cyclic loading are presented. There is a saturation of the stress field near the bottom of the indented crater after the first few cycles of loading. A residual tensile stress field in the direction normal to the target surface exists underneath the indenter in every cycle, which is responsible for the formation of subsurface layer cracks. Results of the coefficient of restitution obtained from the analysis and experiments are also presented.

1. Introduction

This is the second of a two-paper series dealing with the elastic–plastic deformation of metals under repeated impact. In a previous article [1], the work-hardening behaviour and residual deformation of copper during a complete loading–unloading cycle have been examined. In this paper, the finite element method based upon the EPIC IV computer program has been extended to examine the problem of statically cyclic loading. Numerical results of the deformation field have been obtained for loadings up to ten cycles.

2. Method of analysis

The finite element computer program developed for elastic–plastic contact problems [2] has been used for the analysis of repeated impacts on a copper surface up to ten cycles. Deformation of the target material in a region of 5 mm radius has been analysed, while the rigid ball indenter has a radius of 1.5 mm. The region of analysis was represented by 390 axisymmetric triangular elements and 232 nodes. Details of the mesh and boundary conditions can be found in Fig. 1.

The mechanical properties of polycrystal copper are [3]: Young's modulus, E, 1.225×10^5 MPa; Poisson's ratio, ν, 0.35; initial yield stress, Y, 33.32 MPa (3.4 kg mm^{-2}); hardening rate, H', 1.607×10^3 MPa (constant).

The computer program was constructed such that the maximum value of the load for each impact is reached when the work done by the indenter reaches a specified value. The same value of the work was used for all impacts. This boundary condition corresponds to the case of multiple impacts of the same mass and velocity. The program simulates each impact by applying load increments to the target and computing the work done by the indenter for each load increment. Load increments become successively smaller following the adaptive load incrementation scheme explained previously [1]. Increments are adjusted by a scale factor [1] such that the increment is equal to zero when the total work done is equal to 9.5×10^{-7} J. At this moment load increments change sign and unloading starts. The value of the work done in each impact was chosen to be the same as in the previous study of single impacts.

3. Results

The relation between load and indenter displacement is given in Fig. 2 for ten impacts. The discontinuities in the slope of the loading curve 0–a–d are caused by

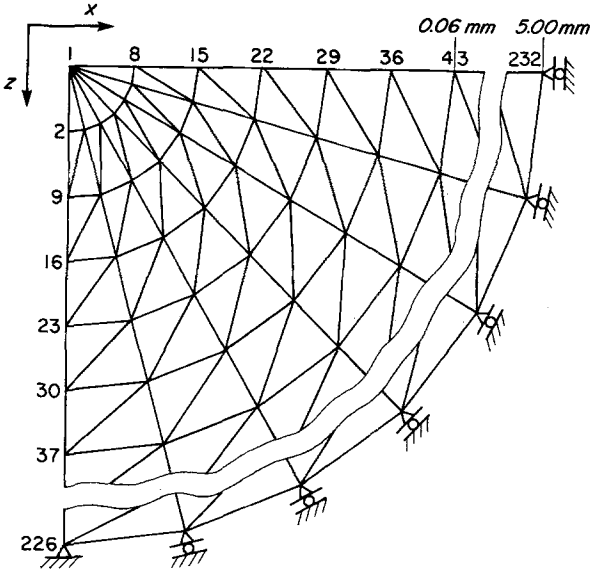

Figure 1 Finite element mesh and boundary constraints. Numbers indicate node number. Radial mesh sizes near origin are 0.01 mm × 6, 0.015 mm × 4, 0.02 × 2, 0.03 × 2, etc.

Permanent address: Department of Mechanical Engineering, University of Electro-Communications, Chofu-City, Tokyo 182, Japan.

0022–2461/87 $03.00 + .12

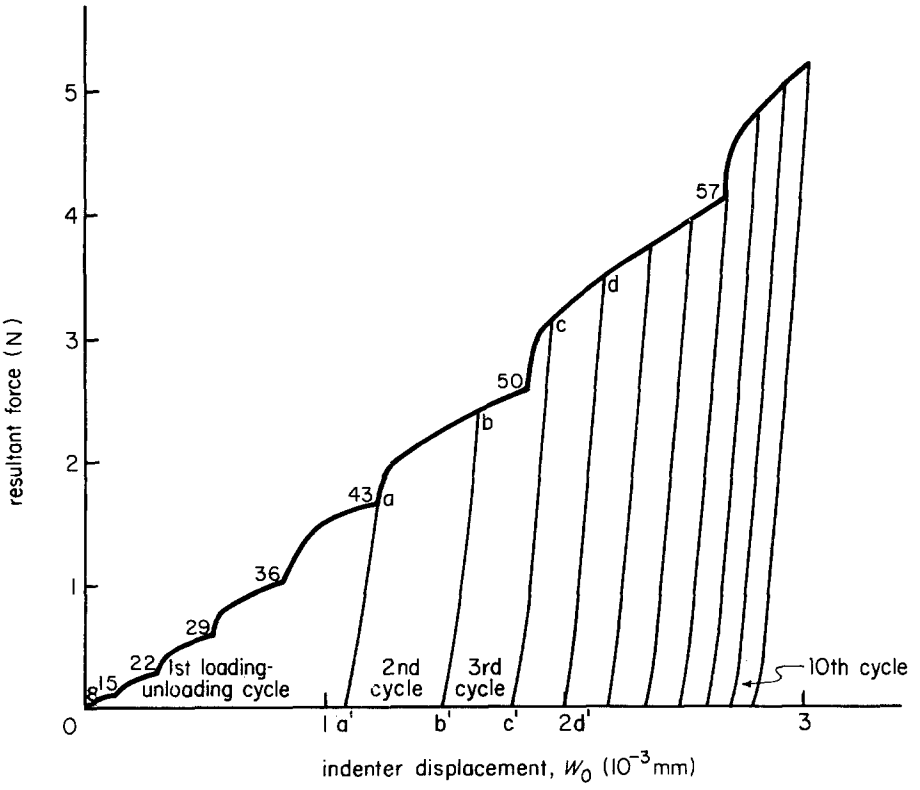

Figure 2 Resultant force plotted against indenter displacement for ten loading–unloading cycles. Numerals on the curve indicate the node in contact with the indenter.

the discontinuous nature of contact of the indenter with the discrete nodal points. Each impact consists of a loading portion and an unloading portion. Line 0a is the loading for the first impact, followed by unloading along aa′. Path a′ab is the loading for the second impact, followed by unloading along bb′. The values of the load for points a, b, c, etc., are the maximum load for each impact. The area under the curve represents the work done by the indenter. Because the work has the same specified value for all impacts, and the maximum load increases as the material hardens, the width of the enclosed area decreases with each successive impact. Fig. 2 shows that the load during a repeated impact rises by following almost the same path obtained from the unloading portion of the previous cycle in the opposite direction, namely a′a, b′b, c′c, etc. A slight hysteresis has been noted from the numerical results but it is too small to be shown in Fig. 2. The hysteresis seems to be due to yielding of some elements during unloading. The resultant change in plastic strain is insignificant.

The displacements of a few representative points in a section of the central region with a radius of 0.14 mm are illustrated in Figs 3 and 4. Each solid line segment

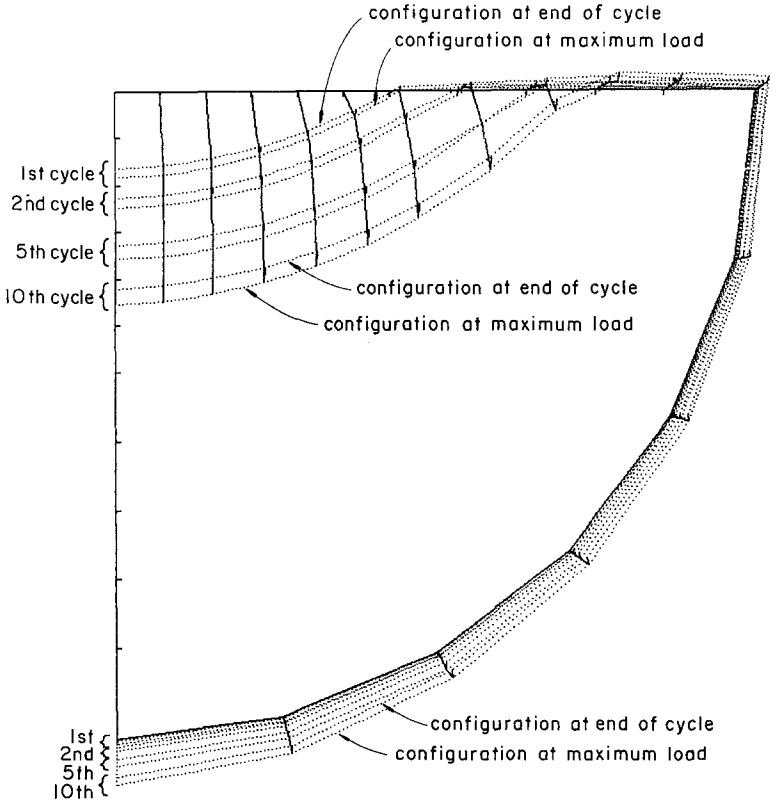

Figure 3 Path of flow of representative points on the surface and the perimeter of a section of the central region. Deformed configuration resulting from that flow at maximum load and at end of cycle for the 1st, 2nd, 5th and 10th cycle. Flow segments and deformation amplified 15 times.

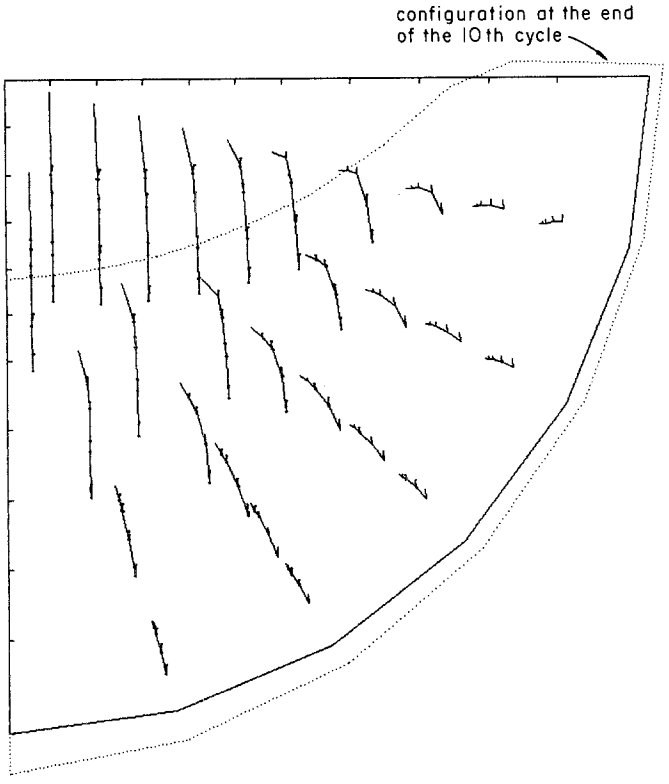

Figure 4 Path of flow of representative interior points in the bulk of a section. Deformed configuration at the end of the 10th cycle. Flow segments and deformation amplified 15 times.

in the field represents the displacement locus of a material point. In Fig. 3, the displacements of points on the surface of the material and along the perimeter of the section for the 1st, 2nd, 5th and 10th cycles are shown. The dotted lines describe the deformed configuration at maximum load, and after unloading, for each cycle shown. The displacements and deformation are magnified 15 times. Therefore, profiles of the crater in Fig. 3 show that they are 15 times deeper than the actual size because horizontal displacements of the surface are sufficiently small. In Fig. 4, the displacements of interior points of the same region as Fig. 3 for the 1st, 2nd, 5th, and 10th cycles are shown. The dotted line represents the deformed configuration after the 10th cycle. Displacements and deformations are magnified 15 times. Fig. 5 shows the detailed features of the displacement segments of Figs 3 and 4. Points A, B, C and D are the positions of material point 0 at the end of the loading portion of the 1st, 2nd, 5th and 10th cycle, respectively. The vertical lines AA′, BB′, CC′ and DD′ indicate the path of unloading as well as the path followed by the initial loading of the subsequent cycle. A displacement vector for any unstressed material point is obtained at any instant by connecting the initial unstressed point 0 and a point on the curve.

Elastic–plastic boundaries at maximum load of the 1st, 2nd, 5th and 10th cycles are shown in Fig. 6. The boundaries are drawn along element mesh lines. The plastic regions grow while maintaining similar shapes.

The contours of constant equivalent stress at maximum load of the 5th and 10th cycles are shown in Figs 7a and b, respectively. In both figures the largest stress appears in the region just inside of contact radius and near the surface. In the region below the centre of the contact surface, work hardening proceeds at a much lower rate than in any other radial direction after the 5th cycle.

In Figs 8 to 15, stress contours are constructed from the stress data at maximum load at each node. The

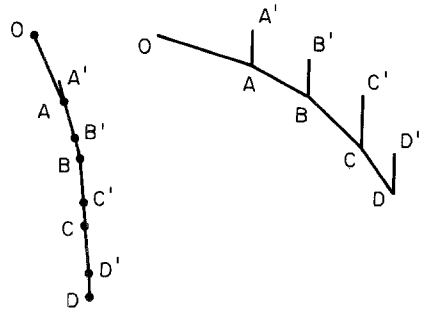

Figure 5 Typical loci of flow of material points.

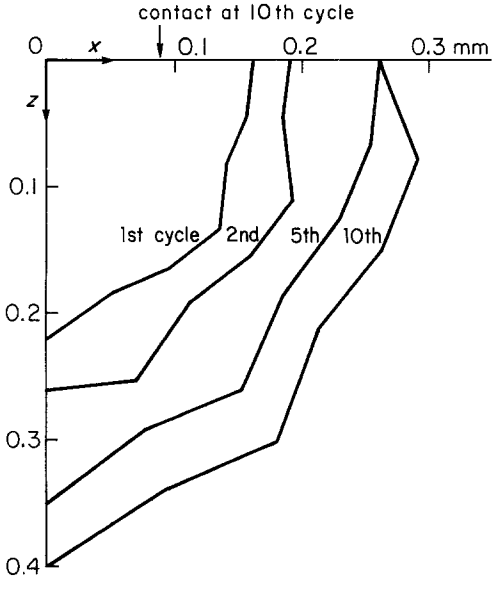

Figure 6 Elastic–plastic boundaries at maximum load of the 1st, 2nd, 5th and 10th cycles.

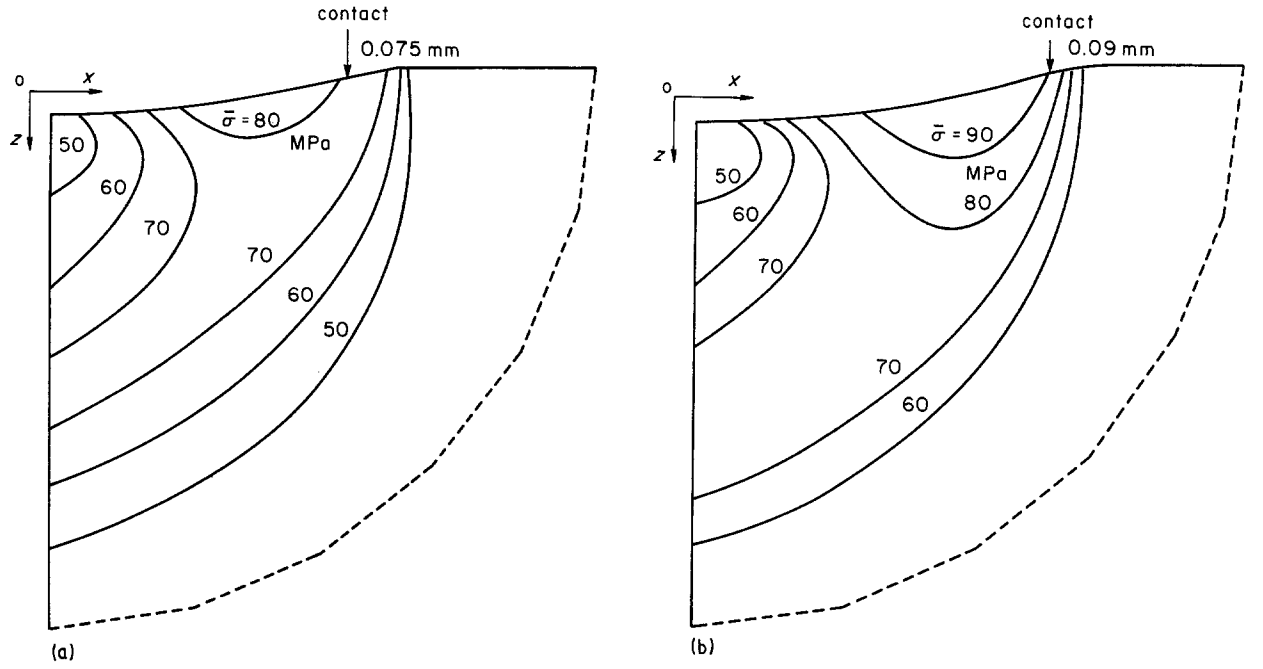

Figure 7 Contours of constant equivalent stress at maximum load of (a) 5th cycle and (b) 10th cycle. The edge of the contact circle is indicated by an arrow.

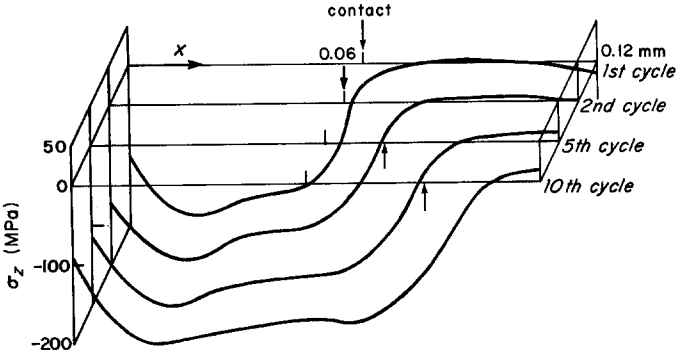

Figure 8 Distributions of σ_z along the x-axis (surface) at maximum load of the 1st, 2nd, 5th and 10th cycles.

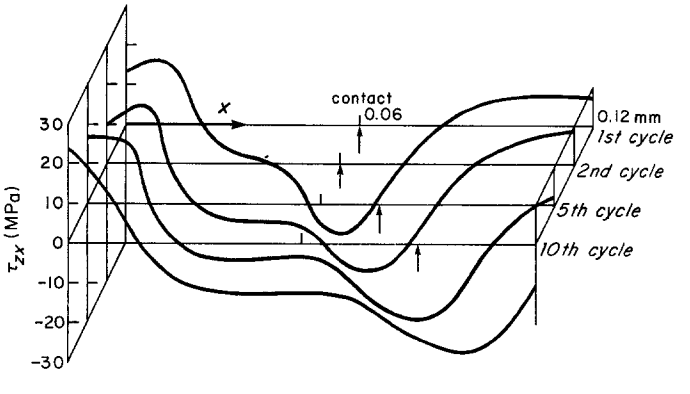

Figure 9 Distributions of τ_{zx} along the x-axis (surface) at maximum load of the 1st, 2nd, 5th and 10th cycles.

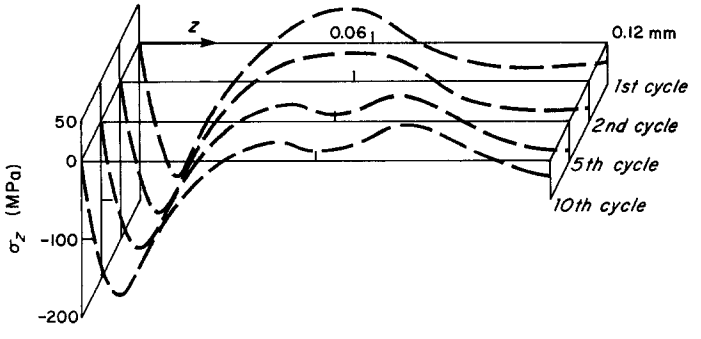

Figure 10 Distributions of residual stress σ_z along the z-axis at the end of the 1st, 2nd, 5th and 10th cycles.

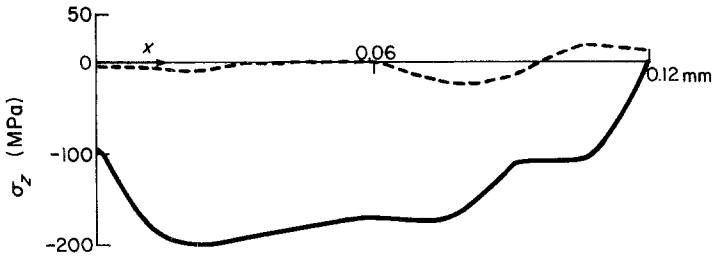

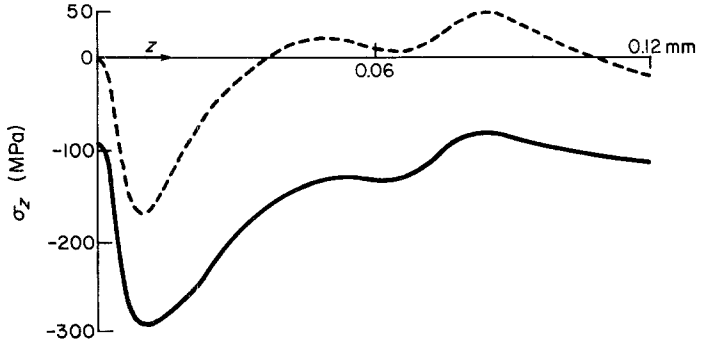

Figure 11 Distributions of σ_z for the 10th cycle at (——) maximum load and (– – –) after unloading along the x-axis and z-axis.

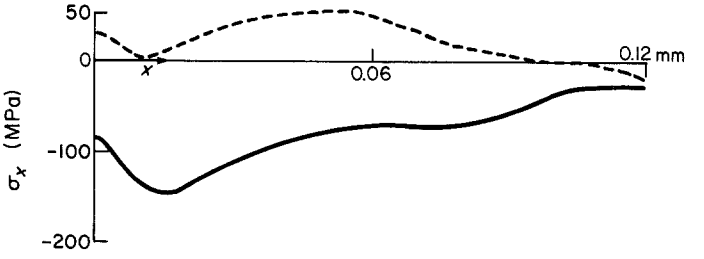

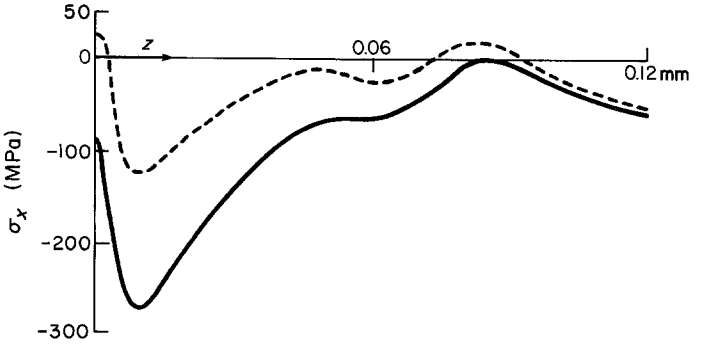

Figure 12 Distributions of σ_x for the 10th cycle at (——) maximum load and (– – –) after unloading along the x-axis and z-axis.

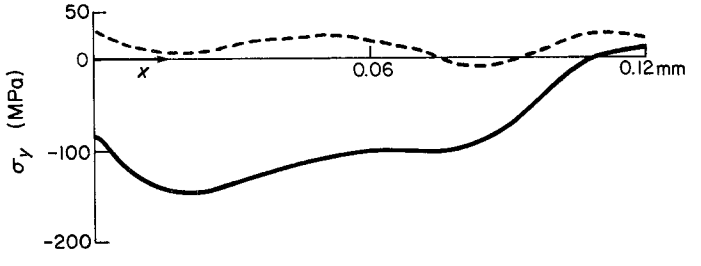

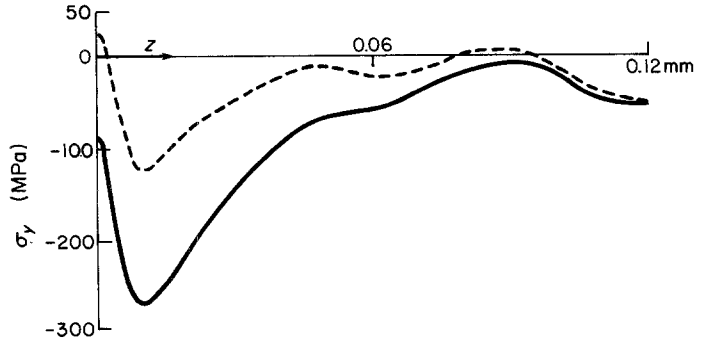

Figure 13 Distributions of hoop stress σ_y for the 10th cycle at (——) maximum load and (– – –) after unloading along the x-axis and z-axis.

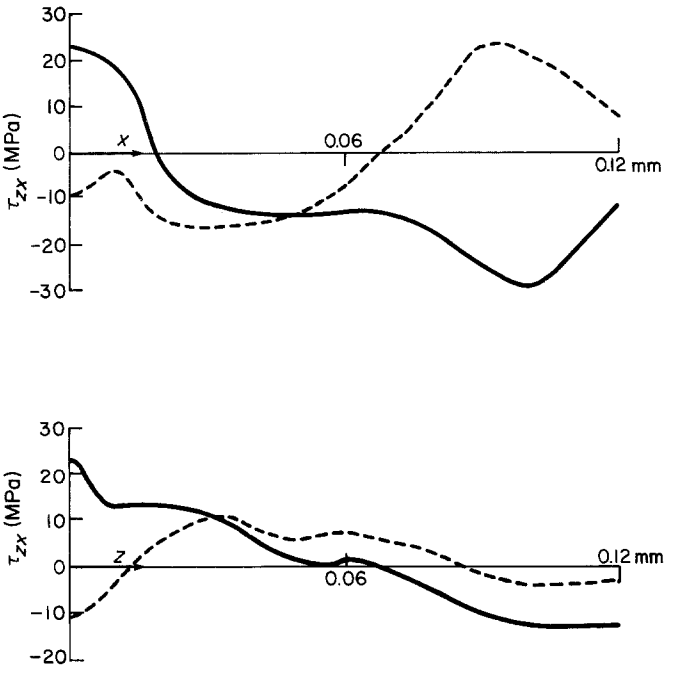

Figure 14 Distribution of τ_{zx} for the 10th cycle at (——) maximum load and (– – –) after unloading along the x-axis and z-axis.

values are the averages of the stresses of elements immediately surrounding a node. Therefore, in Figs 8 to 15 the stress distribution along an axis represents the stress distribution in the vicinity of that axis.

The distributions of σ_z and τ_{zx} in the vicinity of the surface slightly below the x-axis for maximum load in the 1st, 2nd, 5th, and 10th cycles are given in Figs 8 and 9. Fig. 8 shows the distribution of indentation pressure (σ_z) near the contact surface. In each cycle shown, σ_z assumes a minimum value at $x \simeq 0.02$ mm, and changes sign outside the contact area. Fig. 9 shows the distribution of the shear component τ_{zx}. This stress has two peak values; one is positive and occurs near the symmetry axis, and the other is negative and occurs near the contact radius. When the number of cycles increases, the peaks broaden while the peak stresses remain almost constant. The position of the contact radius in Figs 8 and 9 does not change from the 1st to the 2nd cycle because changes are discrete. The contact radius does not change until an additional node comes into contact with the indenter.

Fig. 10 shows the distribution of residual stress σ_z along the z-axis at the end of the loading portion of the 1st, 2nd, 5th and 10th cycles. As pointed earlier [1], a residual compression field is formed directly underneath the contact area. A residual tensile field of minor intensity is produced with its maximum occurring at a depth approximately equal to the contact radius.

Figs 11 to 14 compare the stress at maximum load to the stress after the load is removed for the 10th cycle. The profiles of the residual stress for the normal components σ_z, σ_x and σ_y assume nearly the same general shape as those at the maximum loads. The curves for τ_{zx} in the loaded and unloaded conditions intersect with each other and do not show the same symmetry.

Contours of residual stress σ_z at the end of the 5th and 10th cycles are shown in Figs 15a and b, respec-

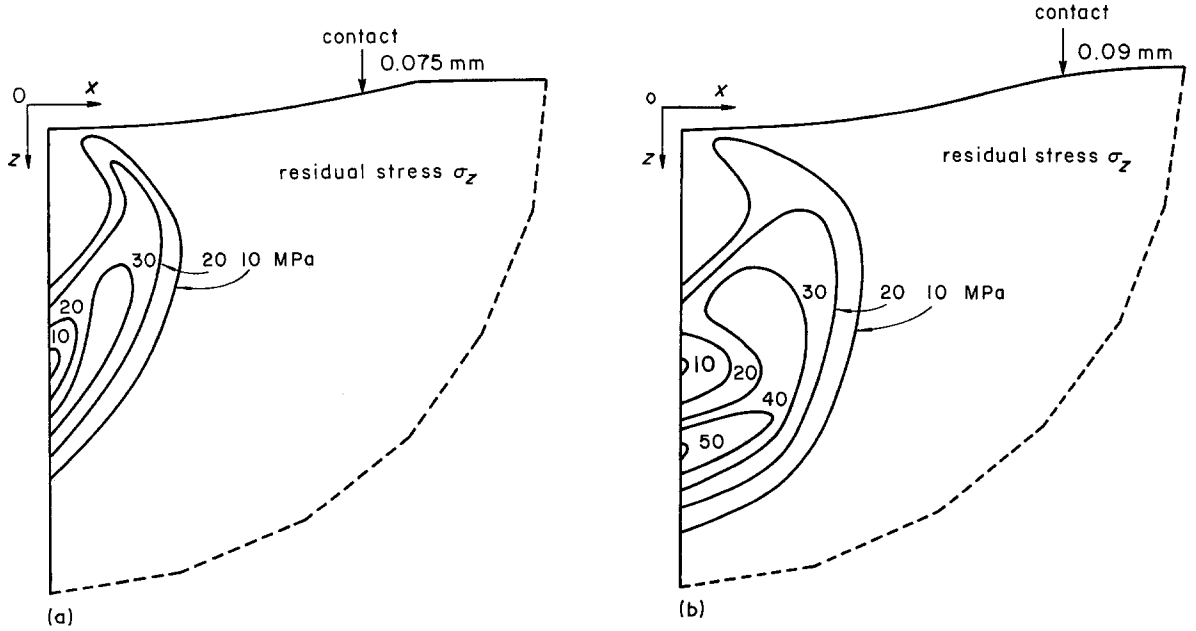

Figure 15 Contours of constant residual stress σ_z at the end of the (a) 5th and (b) 10th cycles.

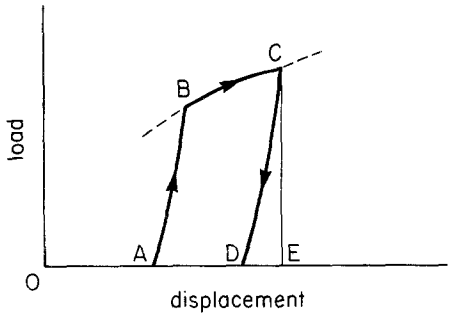

Figure 16 Indenter load–displacement relation for a typical cycle.

tively. Contours for compressive stress are eliminated from the figure. The maximum tensile stress below the center of the indentation appears at a depth from the surface approximately equal to the contact radius.

Finally, the coefficient of restitution for each cycle can be calculated from the knowledge of the elastic field. To obtain the coefficient of restitution, it is assumed that the kinetic energy of the indenter is completely transformed to mechanical work to deform the target material, and that the elastic energy released by the target material at unloading is completely transmitted to the indenter. Consider the indenter load–displacement curve of a typical cycle (see Fig. 16); the work of the indenter or its kinetic energy is given by the area of ABCE, and the elastic energy released by the target material upon unloading is given by CDE. Theoretical values of the coefficient of restitution have been obtained for the ten cycles and the results are shown in Fig. 17. Experimental results [4, 5] have also been included in Fig. 17. The two sets of experimental points were obtained using impact energy equal to 6.3×10^{-3} J and 0.9×10^{-3} J, respectively. The theoretical values, calculated using energy equal to 9.5×10^{-7} J, lie above the experimental points and follow the same general shape. As the

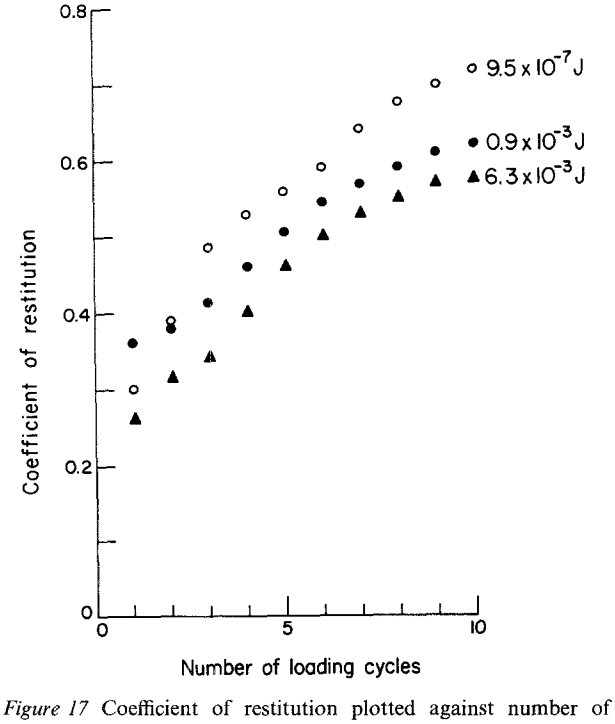

Figure 17 Coefficient of restitution plotted against number of impacts. (▲)(●) Experimental [4, 5], (○) present analysis.

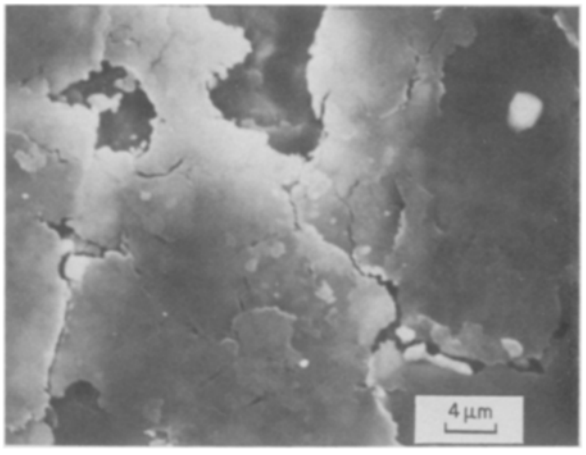

Figure 18 Flaking layer of material at the base of an indentation produced by 10^5 impacts.

number of loading cycles increases from 1 to 10, the difference between the calculated and the experimental values also tends to increase.

A qualitative comparison of analyses with experiments [6] can be made. Fig. 18 shows the flaking and cracking of the surface layer at the base of a crater produced by 10^5 impacts. The normal stresses σ_z of Figs 10 and 11 are believed to be responsible for this damage [5].

4. Discussion and conclusions

1. The state of the stress field near the bottom of the crater at maximum load or complete unloading exhibits only a small change from cycle to cycle after the first few cycles of loading. This indicates a saturation of the stress field.

2. A residual tensile stress field, σ_x, is formed underneath the indenter in every cycle. The position of the maximum residual stress changes gradually with the number of cycles, and it occurs at a distance from the surface approximately equal to the contact radius. The target material at this location is subjected to severe alternating stresses; large compression in the loading phase and tension about the same magnitude as the initial yield stress at unloading. This tensile residual stress field is believed to be responsible for the formation of subsurface layer cracks. (See Iturbe *et al.* [6] for experimental observations.)

3. Results of the coefficient of restitution obtained from the analysis show good agreement with experiments Iturbe and co-workers [4, 5]. However, it should be noted that the analysis and the experiments are conducted for rather different ranges of deformation and that anelastic effects and other energy losses present during the experiments were not included in the calculations. Furthermore, the calculations were performed for a situation of quasi-static loading. Detailed quantitative comparison with experiments ought to take into consideration the difference between static and dynamic yield stresses.

4. A precise prediction of the coefficient of restitution requires the precise knowledge of the property of the target material. The material properties used in the present analysis are based upon those given by McLean [3], and the stress-strain behaviour has been

approximated as linear-hardening. In addition, in the unloading phase, there exists the possibility of yielding by the reversal in the stress state. However, the present theory of plasticity does not include the Bauschinger effect.

Finally, the lack of knowledge of the exact boundary conditions at the contact surface makes it difficult to evaluate accurately the friction force and hence, the coefficient of restitution.

5. Qualitative comparison between experiments and the present analytical results indicate that the flaking of the surface layer observed in experiments is consistent with the stresses obtained from the analysis.

Acknowledgement

This work is supported by the National Science Foundation under grant no. DMR-800 7282.

References

1. Y. YOKOUCHI, I. G. GREENFIELD and T. W. CHOU, *Met. Trans. A* **14** (1983) 2415.
2. Y. YAMADA and Y. YOKOUCHI, "Programming for Elastic–Plastic Analysis by the Finite Element Method": Introducing Program EPIC-IV, Baifukan (1981) (in Japanese).
3. D. MCLEAN, "Mechanical Properties of Metals", (Wiley, 1965) p. 112.
4. I. G. GREENFIELD and E. B. ITURBE, *J. Mater. Sci.* **20** (1985) 4399.
5. E. B. ITURBE, I. G. GREENFIELD and T. W. CHOU, *J. Mater. Sci.* **15** (1980) 2331.
6. E. B. ITURBE, I. G. GREENFIELD and T. W. CHOU, Wear Mechanism in Copper by Repetitive Impacts, in "Wear of Materials", edited by S. Khalal, A. W. Ruff and K. C. Ludema (American Society for Mechanical Engineers, New York, 1981) pp. 685–8.

Received 16 September
and accepted 8 December 1986